Serkan Kangal
Department of Mechanical Engineering,
İzmir Institute of Technology,
Izmir 35430, Turkey

A. Harun Sayı
Department of Mechanical Engineering,
İzmir Institute of Technology,
Izmir 35430, Turkey

Ozan Ayakdaş
Department of Mechanical Engineering,
İzmir Institute of Technology,
Izmir 35430, Turkey

Osman Kartav
Department of Mechanical Engineering,
İzmir Institute of Technology,
Izmir 35430, Turkey

Levent Aydın
Department of Mechanical Engineering,
İzmir Katip Çelebi University,
Izmir 35640, Turkey

H. Seçil Artem
Department of Mechanical Engineering,
İzmir Institute of Technology,
Izmir 35430, Turkey

Engin Aktaş
Department of Civil Engineering,
İzmir Institute of Technology,
Izmir 35430, Turkey

Kutay Yücetürk
Department of Civil Engineering,
İzmir Institute of Technology,
Izmir 35430, Turkey

Metin Tanoğlu[1]
Department of Mechanical Engineering,
İzmir Institute of Technology,
Izmir 35430, Turkey
e-mail: metintanoglu@iyte.edu.tr

Sinan Kandemir
Department of Mechanical Engineering,
İzmir Institute of Technology,
Izmir 35430, Turkey

Bertan Beylergil
Department of Mechanical Engineering,
Alanya Alaaddin Keykubat University,
Antalya 07450,Turkey

A Comprehensive Study on Burst Pressure Performance of Aluminum Liner for Hydrogen Storage Vessels

This paper presents a comparative study on the burst pressure performance of aluminum (Al) liner for type-III composite overwrapped pressure vessels (COPVs). In the analysis, the vessels were loaded with increasing internal pressure up to the burst pressure level. In the analytical part of the study, the burst pressure of the cylindrical part was predicted based on the modified von Mises, Tresca, and average shear stress criterion (ASSC). In the numerical analysis, a finite element (FE) model was established in order to predict the behavior of the vessel as a function of increasing internal pressure and determine the final burst. The Al pressure vessels made of Al-6061-T6 alloy with a capacity of 5 L were designed. The manufacturing of the metallic vessels was purchased from a metal forming company. The experimental study was conducted by pressurizing the Al vessels until the burst failure occurred. The radial and axial strain behaviors were monitored at various locations on the vessels during loading. The results obtained through analytical, numerical, and experimental work were compared. The average experimental burst pressure of the vessels was found to be 279 bar. The experimental strain data were compared with the results of the FE analysis. The results indicated that the FE analysis and ASSC-based elastoplastic analytical approaches yielded the best predictions which are within 2.2% of the experimental burst failure values. It was also found that the elastic analysis underestimated the burst failure results; however, it was effective for determining the critical regions over the vessel structure. The strain behavior of the vessels obtained through experimental investigations was well correlated with those predicted through FE analysis. [DOI: 10.1115/1.4049644]

Keywords: pressure vessel, burst, experimental, validation, analytical, finite element method, metallic, liner

1 Introduction

High-pressure gaseous storage vessels have been used in various fields such as gas plants, power plants, aerospace, and automotive industry with increasing high energy demand. The working pressure of the vessels is ranging from 200 to 1000 bar depending on the application area [1]. Pressure vessels are mainly classified into four categories based on their construction: type-I,

[1]Corresponding author.

Contributed by the Pressure Vessel and Piping Division of ASME for publication in the Journal of Pressure Vessel Technology. Manuscript received January 11, 2020; final manuscript received December 27, 2020; published online February 11, 2021. Assoc. Editor: Akira Maekawa.

full metal construction; type-II, metal liner with a partial composite overwrap; type-III, metal liner with a full-composite overwrap; and type-IV, plastic liner with full-composite overwrap [2]. Among these, type-III and type-IV vessels provide the most practical solution for high-pressure storage vessel industry, especially for mobile applications, due to their relatively lightweight nature.

Metallic liners used mainly for gas impermeability in type-III storage vessels are the focus of this study. For that and weight reduction purposes, the metallic liner wall thickness throughout the geometry of the vessels generally does not exceed 5 mm, and these can be considered as thin-walled structures. In the design of type-III vessels, the geometry of the metallic liner has a significant effect in terms of the layup of the composite layers. Improper design and potential defects/flaws generated during the manufacturing of metallic liner may substantially affect the performance of type-III vessels under high pressure [3]. Various metallic liners for COPVs have been developed by the researchers to meet specific requirements such as low weight, high strength, high stiffness, structural integrity, blockage of diffusion of gases with smaller atomic size, such as hydrogen, impermeability, cost-effectiveness, long service time, less environmental effects, and ease of maintenance, compared to neat metal storage vessels [4–6]. As liner materials, metal alloys such as Al alloys providing relatively higher specific strength and lower cost are generally preferred for on-mobile applications. It was shown that type-III storage vessels having Al liner provided a significant weight reduction with 40% as compared to those of metal vessels (type-I) [5].

There are several analytical studies focused on metallic cylindrical vessels in the literature. The most recent works on Al vessels have generally been published within the studies on type-III COPVs. A number of studies have considered the mechanical behavior of the liner material only in the elastic region to overcome the complexity of nonlinearity of the plasticity [7]. Several studies suggested that the plastic behavior of Al liner should be considered for designing a more compliant type-III COPV to achieve the maximum structural strength [4,5,8–10]. Robert and Kaufman [4] concluded a small percentage of error between experimental tests and the deformation theory of plasticity while determining the structural instability pressure for an overwrapped cylindrical pressure vessel with Al liner. Kabir [5] also studied the Al liners, which were incorporated with a composite part for mainly its load-sharing capabilities, and compared them with a composite shell without a liner. According to their results, the metallic liner remarkably reduced the principal on-axis stress in both circumferential and helical wounded composite layers. In addition to that, the application of variable liner thickness considerably restricted the deformations of the structure. Zheng and Liu [10] performed a study on the stress behavior and burst pressure determination of cylindrical pressure vessel made of carbon fiber/epoxy with Al liner. They conducted the elastoplastic analysis consisting of the power hardening theory and the Hencky equation in the plastic theory to determine the stress behavior of Al liner. According to the plastic solutions, the radial and hoop stresses were found slightly smaller than the elastic solutions in the liner. Liu and Zheng [11] performed a study on the progressive failure using continuum damage mechanics for type-III pressure vessels. Al 6061-T6 alloy was used as a liner material for the COPVs, which was considered to show isotropic and elastoplastic behavior. The maximum shear stress was the failure criterion to monitor the deformations in the liner. It was seen that some parts of the liner exceeded the yield strength and were deformed plastically under 400 bar. The burst pressure of the type-III vessels was found to be within 1250–1260 bar. It can suggest that the burst pressure of liner highly depends on the pressure causing the yielding of the material. Therefore, the burst strength of a liner used for type-III vessel and cylindrical Al only vessel significantly differs due to the addition of a composite part carrying the main loads [10,11]. Since elastoplastic deformation behavior occurs in the event of high-pressure tests due to the accumulation of stress through the yield strength for metallic vessel structure, it is critical to include plastic deformation theory in the analysis. Here, the classic strength-failure criteria, Tresca [12,13] and von Mises failure theories [13], are used to predict whether a failure occurs or not. However, these failure theories should be modified or accompanied in the case of plastic deformation. Power-law hardening theory [10,13,14] and Hencky equation [10] are some of the approaches for this purpose.

Finite element (FE) analysis is an immensely powerful tool for solving physical problems within several disciplines, including structural mechanics [15]. A solution to a complex structural problem may be only possible through FE analysis. Even though a solution may be obtainable, nonlinearities in the physical problems, including material model and properties, geometry, and contact, can enormously increase computational time. In order to decrease computational time/power, some assumptions and simplifications can be made and/or specific analytical approaches may be implemented into the FE solution algorithm using a commercial FE software package such as ANSYS.

In order to predict the burst pressure of a vessel, material properties and elastoplastic models must be determined via experimental validation if possible. Material models for the plastic region of pressure vessel material gain great importance, especially after the maximum load attained (postnecking). Several studies reported in the literature involved different ductile metals. Ling [16] proposed a postnecking plastic behavior model for various alloys and compared it with the power-law using FE analysis. A similar approach was followed by Yao et al. [17] for SAE 304 steel, and the acquired model was applied to different alloys for successful prediction of failure strains for a custom tensile test. The tensile behavior of ductile steel (34CrMo4), which is a widely used material for pressure vessels, was studied through tensile testing of vessel material and FE analysis [18]. A geometric defect implemented through the FE software and Gurson–Tvergaar–Needleman (GTN) model was used for ductile fracture initiation for 34CrMo4 steel. The experimental data were used for the evaluation of GTN model parameters, and a parametric study was performed for geometric defect size. Geometrical imperfections implemented through FE software for a circular casing were also studied [19]. The reliability of the predicted burst pressures of the circular casing was validated through a comparison with a series of experimental burst test data. The postnecking tensile behavior of steel was studied utilizing digital image correction (DIC) experimental setup and the plastic model including the postnecking region was correctly estimated for commercial ferritic steel and dual-phase steel [20]. During metal forming and other processes involving large deformations, resulting metal may exhibit a weak anisotropy. This phenomenon was studied through experiments and FE analysis to obtain the proper material response of Al-6061-T6 at larger strains [21]. With a DIC system that is capable of measuring local strains, tensile and disk compression test data were used for the validation of several anisotropic yield models, and it is reported that the yield function acquired from Barlat et al. [22] demonstrated the most proper behavior to the experimental data. Korkolis et al. [23] performed FE simulations for biaxially (internal pressure and axial) loaded Al 6061-T6 tubular structures. Different yield functions, including von Mises, the nonquadratic Horford, and both isotropic and anisotropic Yld2000-2D, were implemented into the FE code. Numerical simulations were experimentally validated, and it was found that the Yld2000 model, when suitably calibrated, can predict the strains paths for most of the experiments. Xue et al. [24] estimated the burst pressure and location of a cylindrical shell intersection by static and nonlinear (both geometry of deformation and material behavior) FE analysis. Three-dimensional (3D) solid 20 node elements were employed, and multilinear material properties of A672 and A106 steel were input as tabulated data. The model reduction was also performed with the use of two symmetric planes. It is experimentally found that the developed FE model predicted both burst pressure and location well. Brabin et al. [25] compared several predictive equations for determining the burst

Table 1 Mechanical properties of the Al 6061-T6 [26]

Symbol	Description	Unit	Value
E	Young's modulus	GPa	67.29
v_{12}	Poisson's ratio		0.33
σ_y	Yield strength	MPa	269.85
$\sigma_{ult,\ true}$	True ultimate tensile strength	MPa	325.79

pressure of different types of mild steel. Comparisons with experimental findings were made, and it was found that Faupel formula provided the best predictions for the test results. It was also noted that no single failure criterion could predict accurately for different types of materials and geometries.

As one can see, the burst pressure predictions for metal-based pressure vessels were abundant in the literature. However, the number of studies considering a comparison of experimental, numerical, and analytical burst pressure and location of Al-6061-T6 pressure vessels suitable for type-III composite overwrapped high-pressure hydrogen gas storage systems is limited. In this regard, this study aims at filling the gap in the literature and revealing the potential for comparison of the methods. Neat Al-6061-T6 pressure vessels were experimentally investigated through both tensile and burst pressure testing. Calculations of various analytical approaches have been carried out for the prediction of burst pressure, and an FE model was established in order to predict the behavior of the vessel while increasing the internal pressure and final burst pressure. The main objective of this study is to compare the experimental, numerical, and analytical burst pressure findings and observe the mechanical behavior while internally pressurizing the Al vessel by FE analysis and experimental testing.

2 Materials and Methods

The pressure vessels made of aluminum 6061-T6 with a capacity of 5 L were designed. The tensile properties of aluminum are given in the literature as in Table 1. The design and dimensions of the manufactured vessels are represented in Fig. 1. The manufacturing of the vessels was conducted by a metal forming company (Sima Foreign Trade, Aluminum Industry Inc.) based in Turkey. The aft dome was shaped with deep drawing while the front dome of the vessel was given its final form with spinning. The manufactured vessels were seamless. An example image of the manufactured vessel is shown in Fig. 2.

2.1 The Mechanical Properties of the Pressure Vessel Material. In order to determine the mechanical properties of the Al vessel, tensile tests were performed according to ASTM E8/E8M—16a standard [27]. For this purpose, tensile test specimens were obtained from the cylindrical section of a manufactured Al vessel using a water jet according to ASTM E8M (Fig. 3(*a*)). Speed of testing was determined according to the ASTM E8M-16a Control Method C. 2 mm/min crosshead speed was selected which produces a rate of straining 0.033 mm/mm/min. The strain measurements were obtained utilizing a video extensometer. Five specimens were tested at room temperature. The tensile properties that were obtained from testing were Young's modulus, Poisson's

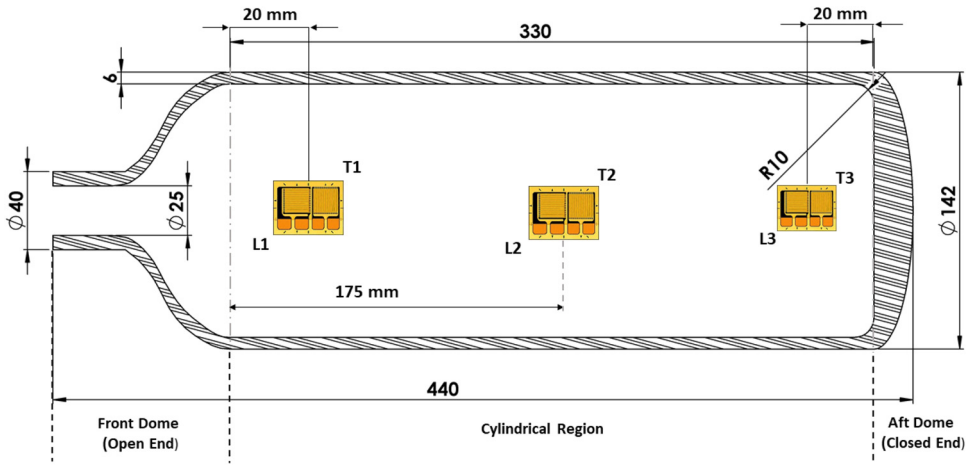

Fig. 1 The design of Al-6061-T6 vessels developed within the research (dimensions are in mm) with representative strain gauge positions

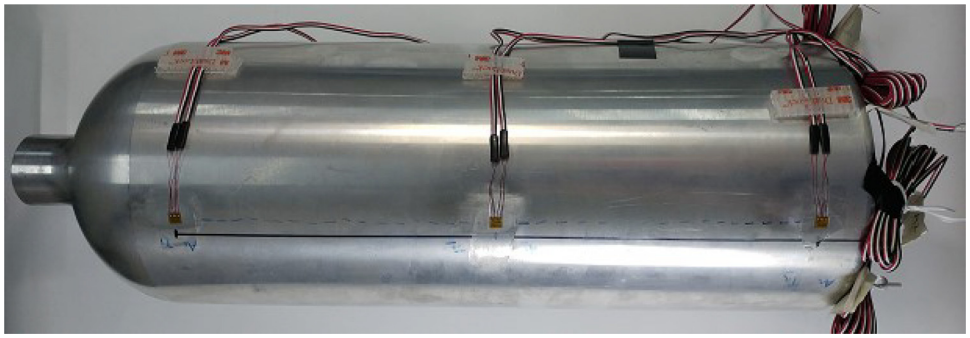

Fig. 2 Photograph of the Al liner with mounted strain gages prepared for burst testing

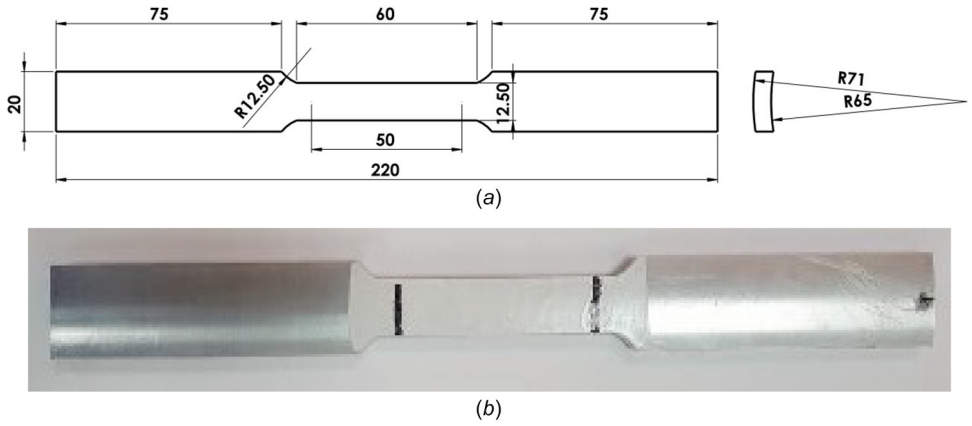

Fig. 3 (*a*) The dimensions of a tensile test specimen (*b*) photograph of a tensile test specimen sectioned from the Al vessel, in accordance with ASTM E8/E8M—16a

ratio, yield strength, and ultimate tensile strength. Also, bilinear isotropic hardening tangent modulus, fracture strength, fracture strain, and strain hardening exponents were calculated from the stress–strain behavior of the test specimens. The average values of the results with corresponding standard deviations were reported.

The true stress–strain data after yielding is needed for determining the plastic behavior of Al 6061-T6 in ANSYS software package. For this reason, the experimental engineering stress–strain data were converted into the true stress–strain data up to the necking point, assuming that uniform deformation occurs until that point.

2.2 Burst Pressure Testing of the Al Vessel. The burst pressure values of Al pressure vessels were measured by the hydrostatic pressure test. Internal hydrostatic pressure was applied to the vessels up to burst failure. Moreover, during the burst pressure test, the local strain values on the surface of the vessels were measured using strain gages. Three strain gages were used to determine radial and longitudinal strain values during burst pressure tests. The strain gages at their exact locations are shown in the technical drawing and test specimen (Figs. 1 and 2).

2.3 Analytical Approaches for Burst Pressure Prediction. Stress analysis and burst pressure predictions of the Al vessel were investigated analytically for the dome and the cylindrical sections. Since it is not possible to perform analytical calculations with a single formula throughout the pressure vessel, the burst pressure calculations of the pressure vessel were done for the dome and cylindrical sections, separately. For a considerably safer design of the vessel, the burst failure is not expected at the dome section of the vessel. Therefore, analytical calculations were performed in two steps, namely: (i) elastic analysis of both dome and cylindrical section and (ii) elastoplastic analysis of the cylindrical section to determine failure initiation to obtain more accurate results. This procedure was a common way to overcome the complexity in the analytical studies [12,25,28–30]. In the elastic analysis, the prediction of the burst pressure was based only on the elastic behavior of the material.

In the elastoplastic analysis, the plasticity of the vessel material after the yielding was also considered in the calculation of the burst pressure. The elastic and elastoplastic stress and failure analysis of the Al vessel have been carried out based on the theories for thin-walled pressure vessels, modified Tresca and von Mises solutions.

2.3.1 Elastic Analysis. In the analysis of elastic burst pressure calculation of the Al vessel, the dome section of the vessel is considered to be ellipsoidal. The sections of the vessel, geometric properties, and stress components used in the stress analysis of the dome section are given in Fig. 4. The parameters (t, R, D, R_L, R_m, h, r, L, X) in Fig. 4 represent wall thickness, radius of the cylindrical section, diameter, latitudinal radius of the curvature, meridional radius of the curvature, depth of head, knuckle radius, crown radius, and the location of a point on the surface of the dome section measured from the centerline, respectively. The meridional, σ_x and latitudinal stress, σ_ϕ components in terms of internal pressure P, for both dome and cylindrical sections of the vessel, were calculated by using the expressions given in Table 2 [31].

where

$$R_L = \sqrt{R^4/h^2 + X^2(1 - R^2/h^2)}, \quad R_m = R_L^3 h^2/R^4 \quad \text{at any point } X \tag{1}$$

$$R_m = R_L = R^2/h \quad \text{at the center of the dome} \tag{2}$$

$$R_m = h/R, \quad R_L = R \quad \text{at the tangent line} \tag{3}$$

2.3.2 Elastoplastic Analysis. The prediction of the burst pressure of the metallic cylindrical vessel is of critical importance for a safe design. Since, the burst pressure, also called as failure pressure or limit load at plastic collapse, determines the maximum load-bearing capacity of the vessel. Al 6061-T6 used as the vessel material is a power-law hardening material, similar to the majority of the common metals. Therefore, analytical approaches for predicting the plastic collapse of a metallic thin-walled vessel featuring the plasticity of the material were taken into consideration [28].

The theories predicting the burst pressure are (i) Tresca-based approach, which provides a lower bound and (ii) von Mises-based approach providing an upper bound to the burst pressure. Moreover, a new multi-axial yield criterion called average shear stress criterion (ASSC), first proposed by Zhu and Leis [28], is likely to predict the burst pressure more accurately than the theories based on traditional ones. In the analysis, Tresca-based theory, von Mises-based theory, Svensson's simplified solution, Christopher's solution, and ASSC-based theory were carried out.

In the Tresca-based approach, the Tresca yield criterion is applied to the plastic flow theory with the use of stress–strain constitutive relation and Tresca equivalent strain. Thus, the burst pressure based on Tresca criterion can be expressed as [28]

$$P_b = \left(\frac{1}{2}\right)^{n+1} \frac{4t}{D_m} \sigma_{\text{ult}} \tag{4}$$

where D_m is the mean diameter, t is the wall thickness, and n is the strain hardening exponent for the power-hardening materials expressed as [32]

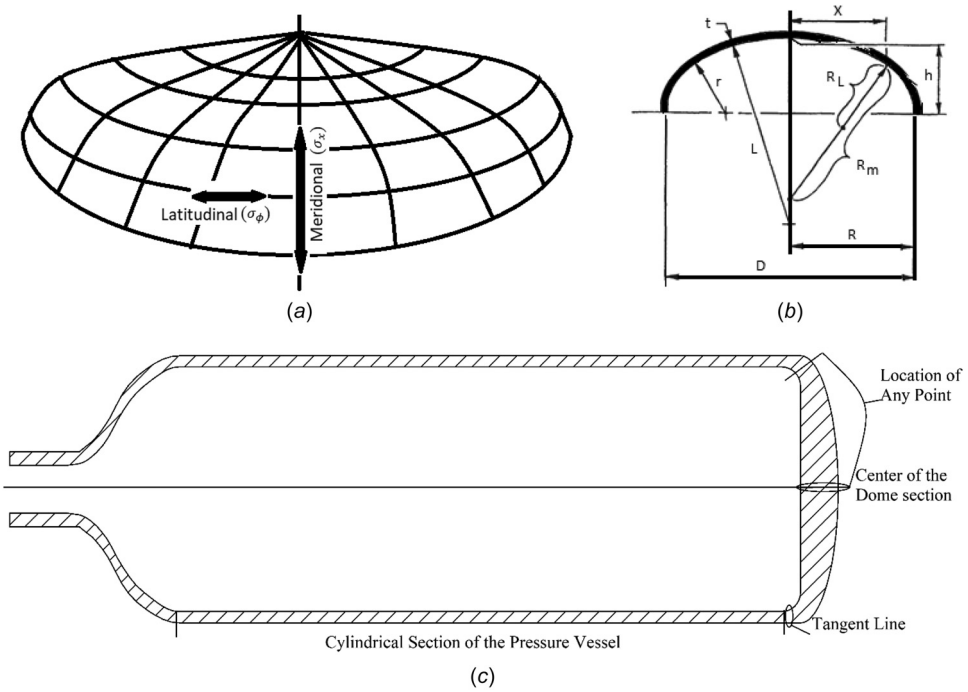

Fig. 4 (*a*) Stress directions in the dome section [31], (*b*) dimensional parameters in the dome section [31], and (*c*) the sections of the Al pressure vessel

Table 2 Stress components of the pressure vessel for described locations

	σ_x	σ_ϕ
At any point X	$PR_L/2t$	$PR/t(1-R_L/2R_m)$
At the center of the head	$PR^2/2th$	$\sigma_x=\sigma_\phi$
At the tangent line	$PR/2t$	$PR/t(1-R^2/2h^2)$
At the cylindrical section	$PR/2t$	PR/t

$$n=\frac{\log\left(\frac{\sigma_f^3\sigma_{\text{ult}}^2}{\sigma_{\text{ys}}^5}\right)}{3\log(500\varepsilon_f)} \tag{5}$$

In Eq. (5), σ_{ult}, σ_f, σ_{ys}, and ε_f define the maximum tensile strength, failure strength, yield strength, and failure strain, respectively.

Similarly, using the von Mises equivalent strain and the stress–strain constitutive relation, the von Mises criterion is applied to the plastic flow theory. The solution for the burst pressure is then defined as [28]

$$P_b=\left(\frac{1}{\sqrt{3}}\right)^{n+1}\frac{4t}{D_m}\sigma_{\text{ult}} \tag{6}$$

The burst pressure obtained with ASSC embeds a weighted average of the stress based on Tresca and von Mises criteria. This new theory is known to improve the burst pressure estimation of the flow response from the elastic domain into and through elastic–plastic response for thin-walled defect-free cylindrical pipes and vessels.

The burst pressure predicted based on ASSC can be expressed as [28]

$$P_b=\left(\frac{2+\sqrt{3}}{4\sqrt{3}}\right)^{n+1}\frac{4t}{D_m}\sigma_{\text{ult}} \tag{7}$$

Another analytical solution to plastic instability for both thin- and thick-walled cylindrical vessels based on von Mises yield criterion is so-called Svensson's simplified solution [30], expressed as

$$P_b=\sigma_{\text{ult}}\left(\frac{0.25}{n+0.227}\right)\left(\frac{e}{n}\right)^n\ln\left(\frac{D_0}{D_i}\right) \tag{8}$$

where e is the Euler's number, D_0 is the outer diameter, and D_i is the inner diameter of the cylindrical vessel.

Christopher et al. [30] proposed a solution based on von Mises yield criterion for specifically thin-walled cylindrical vessels. In this approach, the expansion of cylindrical vessel in an axial direction is assumed to be negligible to its length, the material is incompressible at the beginning of plastic instability, and the area of the cross section remains the same before and after deformation. Following the definition of Christopher et al., the burst pressure is estimated as

$$P_b=\frac{2}{(\sqrt{3})^{n+1}}\frac{t}{R_i}\sigma_{\text{ult}} \tag{9}$$

where R_i is the inner radius of the cylindrical vessel.

2.4 Finite Element Analysis—Validation of the FE Model. A 3D model was created from the dimensions measured from the water jet sectioned specimens for tensile testing. The grip regions were removed to avoid unnecessary inclusion of contact regions with universal testing machine grips and shear loading to the FE analysis. A mesh was formed by using 20 node hexahedral elements with an average size of 3 mm. The resulting 3D mesh of the tensile test specimen model is shown in Fig. 5. One end face on x-direction was defined as a fixed region. 10 mm displacement on x-direction was applied to the other end face on x-direction to observe the postnecking behavior of the tensile specimen (Fig. 5).

Al 6061-T6 material was defined as an elastoplastic material in ANSYS 17.2. Two different isotropic hardening models were utilized for defining the plastic region of the material, the bilinear, and multilinear isotropic hardening [33,34]. The true stress–true strain behavior of Al 6061-T6 was acquired from the experimental tensile testing of the material, and by converting the engineering stress–strain curves up to the necking point calculated elastic

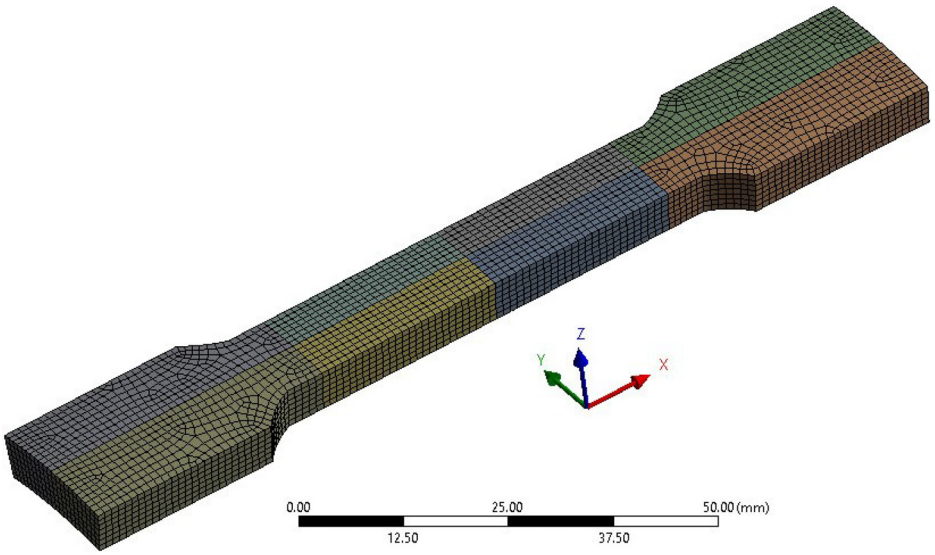

Fig. 5 Tensile testing specimen FE solid model

Table 3 Mechanical properties of the Al 6061-T6 specimens used for FE simulations and analytical calculations

Symbol	Description	Unit	Average value ± standard deviation
E	Young's modulus	MPa	57,548 ± 1328
v_{12}	Poisson's ratio		0.33 ± 0.01
σ_y	Yield strength	MPa	240.3 ± 4.3
$E_{\tan}$	Bilinear isotropic hardening tangent modulus	MPa	975 ± 37
$\sigma_{\text{ult, true}}$	True ultimate tensile strength	MPa	317.0 ± 7.2
$\sigma_{f,m}$	Mean fracture strength	MPa	298.3 ± 5.8
$\varepsilon_{f,m}$	Mean fracture strain	MPa	0.17 ± 0.01
n	Strain hardening exponent	—	0.0896 ± 0.0048

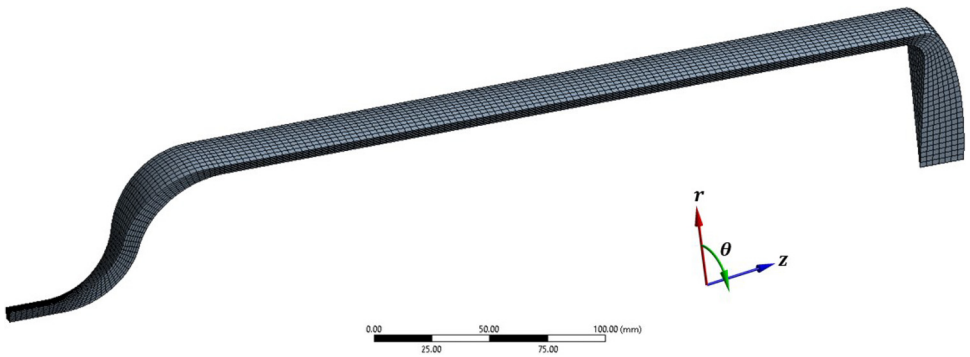

Fig. 6 FE model of the Al vessel with load and boundary conditions

modulus, yield strength, and tangent modulus of the bilinear isotropic model were tabulated in Table 3.

Large deformations were expected as it was intended to observe the postyielding behavior of the materials, so large deformations setting was enabled in the FE analysis software. The displacement as the loading condition was applied linearly until the final time of 1 s, which corresponds to 10 mm of displacement in the x-direction, with three different time-step regions. These time-step regions defined as 0.008 s up to 0.35 s, 0.001 s between 0.35 s and 0.58 s, and finally 0.0005 s until the last converged time-step. It was intended to gradually reduce the time-steps for improving the convergence of the numerical analysis and higher resolution of mechanical behavior through the loading.

2.5 Finite Element Analysis of Al Pressure Vessel. For pressure vessel FE analysis, a solid mechanical model was formed utilizing the aforementioned technical drawing (Fig. 1) and 20 node hexahedral elements (SOLID185 in ANSYS). In order to decrease computation time by taking advantage of axisymmetry, a mesh convergence and a model reduction analysis were performed. Therefore, the model was reduced to half, quarter, and 1/16 of the full 3D model and shown in Fig. 6.

Contact regions with testing apparatus were considered as fixed boundaries and shown in Fig. 7(*a*). The reduced model's both side section boundaries were given as free movement through axial and radial directions but restricted in an angular direction; thus, it is assumed that no rotational motion occurs through the vessel while internally pressurizing it (Fig. 7(*b*)). Finally, the pressure was applied normal to internal surfaces of the pressure vessel except the regions in contact with the testing apparatus.

The mesh convergence study was also performed on the 1/16 model of the vessel. Average element sizes of 2 to 7 mm were

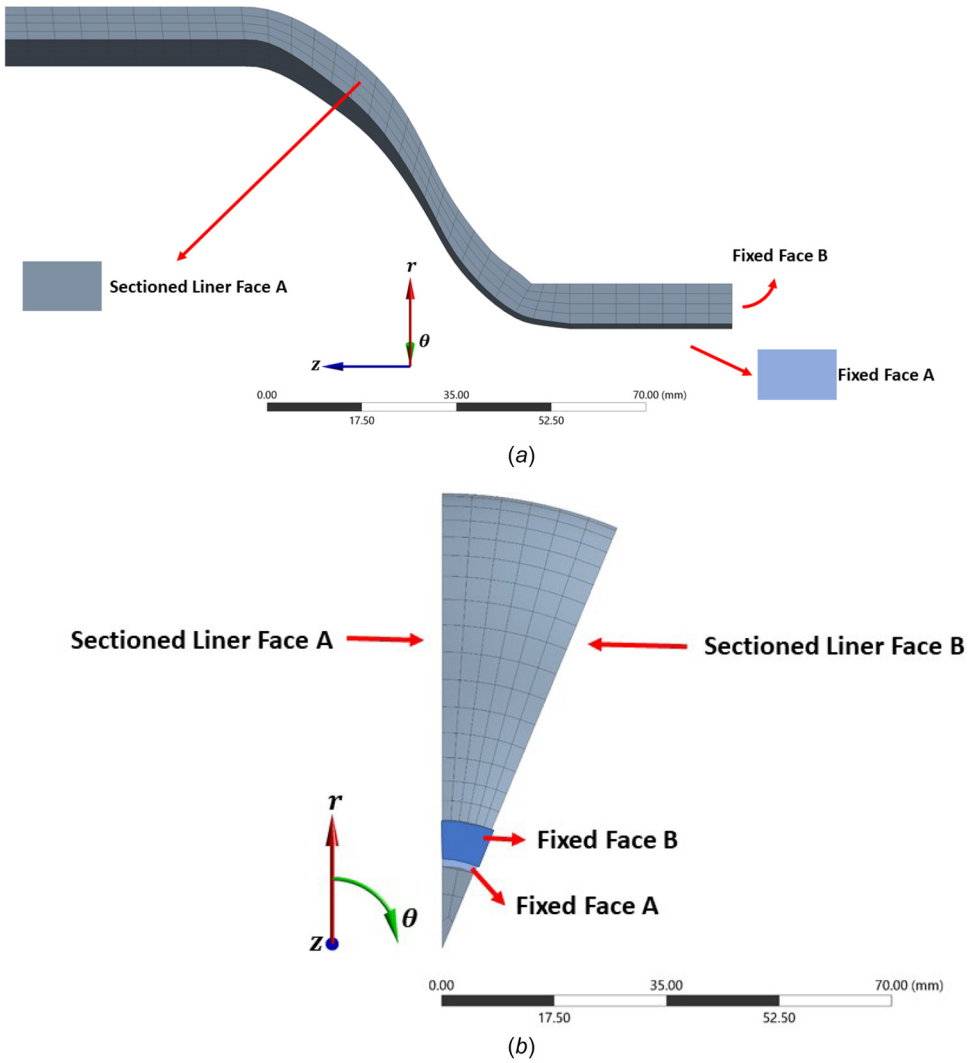

Fig. 7 Boundary conditions for pressure vessel 3D FE model, (*a*) left-view and (*b*) front-view

selected. Below 2 mm element size, it was observed that the mesh is not manageable to work within the ANSYS software. Similarly, above 7 mm element size, severe defeaturing of the model was observed. Furthermore, element size larger than 7 mm had a sizably distorted aspect ratio, in order to ensure that at least three elements were present at the thickness direction, which adversely affects the convergence of the FE analysis.

Analysis settings were configured for the burst pressure simulations similar to the tensile testing numerical model, except the loading was given as pressure instead of displacement, due to the nature of the structural problem. Pressure as a load condition ensures that the force was always applied normal to the surface even in the expected cases of shape change of the surface. This loading condition perfectly represents the case of pressurizing the Al vessel. Loading was applied linearly up to the final calculation time of 1 s, which corresponds to 30 MPa, with four different time-step regions, for improving the convergence of the analysis, thus proper burst pressure calculations of the vessels. Timestep regions were given as follows; 0.008 s up to 0.35 s, 0.002 between 0.35 s and 0.85 s, and finally 0.0005 until last converged timestep. All FE simulations were performed on a Dell Precision WorkStation T7500 featuring 2× HexaCore Intel Xeon X5690 at 3600 MHz and 48 GB of DDR3-SDRAM.

Burst pressure was determined from the load versus deformation behavior of the vessel. Similar to the tensile testing, load versus strain behavior of bilinear and multilinear isotropic hardening models was investigated. The double elastic slope and tangent intersections of elastic and plastic region methods are the two of the methods present in the literature to find the limit pressure. In tangent intersection method, one tangent line drawn to the elastic region and one tangent line drawn to the plastic region of the curve and the burst pressure can be determined intersections of these lines. In double elastic slope method, a straight collapse limit line is drawn from the origin of the load versus deformation curve with the twice slope of the initial elastic response line [35].

3 Results and Discussion

3.1 Experimental Findings

3.1.1 Mechanical Behavior of the Vessel Material. The average mechanical properties of the Al-6061-T6 specimens determined experimentally are given in Table 3. These results measured were employed in further FE analysis and analytical calculations. The engineering stress–strain behavior of the Al specimens under tensile loading is shown in Fig. 8.

3.1.2 Burst Pressure Testing. The burst pressure testing of Al vessels was carried out utilizing the experimental setup described in Sec. 2.2, with strain measurements on three different regions of the vessels. The average burst pressure of Al vessels was measured to be 279 bar. The typical burst failure mode of the vessel is

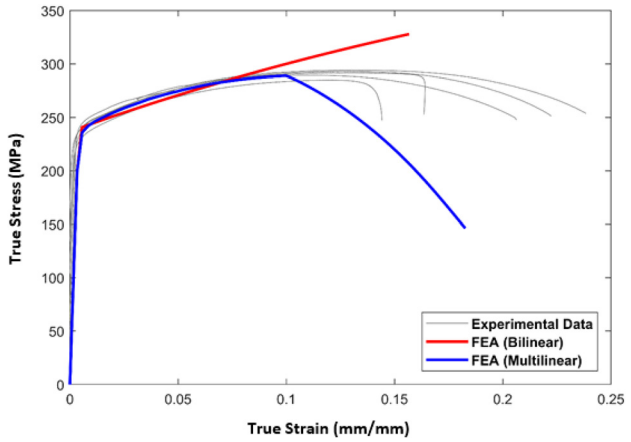

Fig. 8 Stress versus strain curves of the Al-6061-T6 specimens obtained based on tensile testing and FE analysis

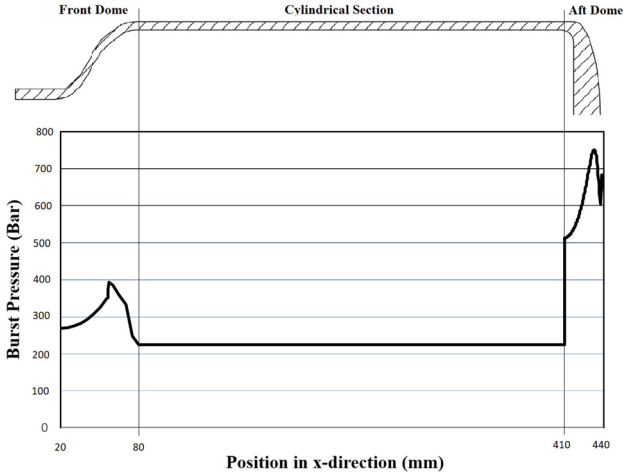

Fig. 10 Analytical burst pressure variation throughout the axial distance of Al vessel

visualized in Fig. 9. As seen in the image, the vessels were failed with the final rupture along the cylindrical section, which is a safe burst mode for those structures.

3.2 Analytical Approaches

3.2.1 Elastic Analysis. Based on von Mises yield criterion and using the stress components for thin-walled Al vessel subjected to internal loading (Table 2), the burst pressure was determined. The variation of burst pressure throughout the length of vessel is given in Fig. 10. It can be seen from the figure that the minimum burst pressure value in front dome was obtained as 269.3 at a point of transition from boss to dome region of the vessel. In the front dome region, the limit load was increased to about 400 bar, followed by a sharp decrease to 224.5 bar while approaching to the cylindrical section. A similar pattern was observed at the aft dome of the vessel. With the increasing wall thickness at the aft dome, limit loads reached to about 750 bar. The limit load for the center of the aft dome was calculated as 682.4 bar. As a result of these elastic region only calculations, the minimum burst pressure has been found to be 224.5 bar at the cylindrical section of the pressure vessel. From these results, it can be concluded that the critical region is a cylindrical part in terms of strength and it was considered that the burst would occur in the cylindrical section of the vessel.

3.2.2 Elastoplastic Analysis. The cylindrical part of the Al vessel also required elastoplastic analysis to determine the failure initiation mentioned previously.

Table 4 summarizes the predictions obtained based on, more generally, Tresca, ASSC, and Von Mises criteria. In this study, estimation by formulae based on the Tresca criterion predicted

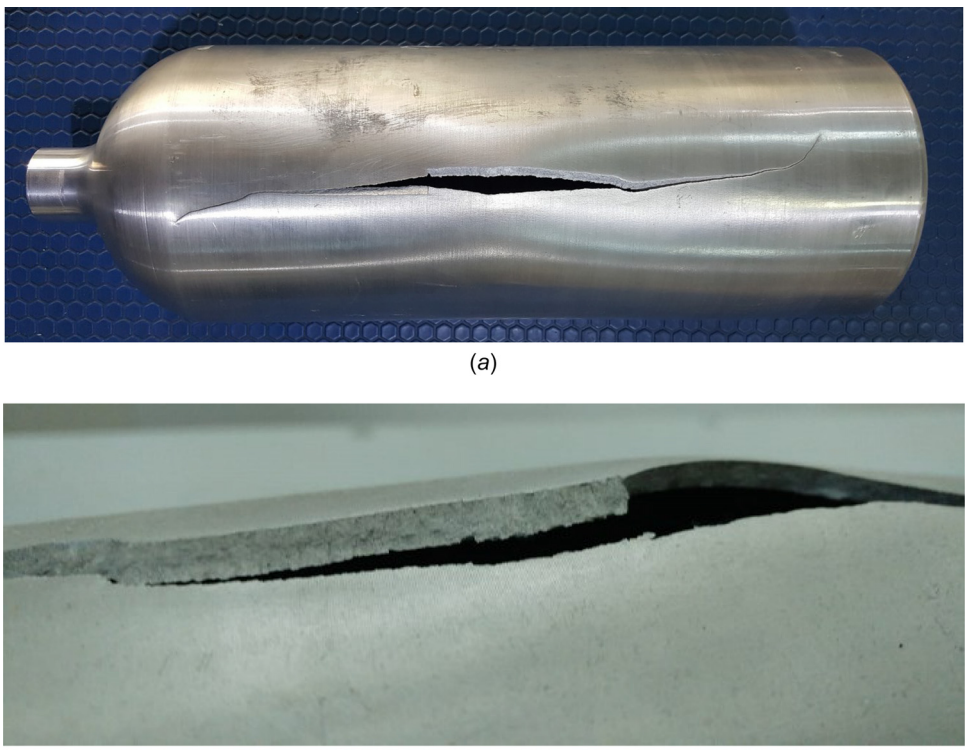

(*a*)

(*b*)

Fig. 9 (*a*) Al pressure vessel after the burst pressure testing and (*b*) the fractured surface

Table 4 Comparison of analytical, numerical, and experimental burst pressure

	Burst pressure, P_b (bar)	Relative error (with respect to experimental result) (%)
Tresca-based	262.8	−5.8
ASSC-based	285.1	2.2
von Mises-based	307.5	10.2
Christopher	321.6	15.3
Svensson's simplified	300.0	7.5
FE analysis bi-linear (excessive strain/end of conversion)	298.55	7
FE analysis multilinear (excessive strain/end of conversion)	257.72	−7.6
Experimental result	279.0	—

Table 5 Comparison of FE models developed for determining the burst pressure

Model size	Average element size (mm)	# of nodes	# of elements	CPU time (s)	Burst pressure (bar)
Full	7	49,492	25,228	1731	257.72
Full	5	170,647	103,108	10,411	257.72
Half	5	34,489	7027	970	257.55
Quarter	5	29,480	5313	842.5	257.55
1/8	5	15,385	2688	375.8	257.55
1/16	5	13,428	2492	354..6	257.55

burst pressure lower than experimental burst pressure. On the other side, the estimations based on von Mises criterion (von Mises-based, Christopher and Svensson's Simplified) remained above the experimental result. The solution based on ASSC estimated the value between Tresca and von Mises criteria based theories as expected [28]. ASSC provided the closest burst pressure prediction to the experimental burst pressure. Relative error was significant in the estimation obtained by Christopher formulation, specifically derived for thin-walled pressure vessels having wall ratio (wall thickness/inner radius) around 1/20. However, the metallic vessel considered in this study has a wall ratio of 1/11. This might have negatively affected the prediction.

3.3 FE Analysis—Tensile Testing. FE material model validated through simulation performed with different boundary conditions and hardening models. Figure 8 shows the comparisons between experimental data and FE analysis. As one can clearly see, the multilinear isotropic hardening model fits well with the experimental results compared to bilinear isotropic hardening.

Two different loading conditions were also compared. Load given as a displacement in x-direction fits well even beyond $\sigma_{\text{eng, UTS}}$. Local deformation at the center of the specimen was also observed in postprocessed results in ANSYS. On the contrary, directly given forces on the same boundary result in convergence problems in ANSYS after $\sigma_{\text{eng, UTS}}$. The load condition given in force or pressure must monotonically increase equivalent stresses in 3D elements in ANSYS. Up to $\sigma_{\text{eng, UTS}}$ both load conditions showed nearly identical behavior. Unfortunately, it is not always possible to give load conditions as displacements as such in the case of internally pressurized vessels.

3.4 FE Analysis—Burst Pressure Testing. Numerical simulations for determining the burst pressure of the Al vessels were carried out for different models. Model specifications such as average element size of meshing, number of nodes, and elements with the corresponding computation time were compared in Table 5.

It can be clearly seen from the burst pressure and mechanical behavior that the structural problem does not have a mesh size dependency at the modeled mesh size level. Moreover, when compared to the full model, the boundary conditions introduced with the model reduction did not affect the mechanical behavior of the vessel. In Fig. 11, axial and radial deformation behaviors of the

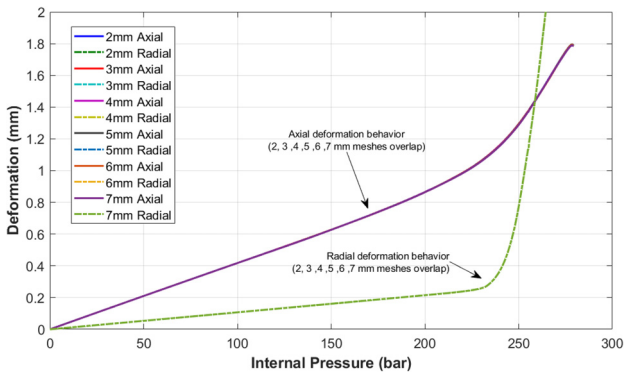

Fig. 11 Radial and axial deformation comparison of FE models with different average element size

vessels with different mesh sizes were compared, and it was found that the deformation curves overlapped on each other seamlessly.

The strain behavior and the elongation of the bilinear and multilinear hardening models were significantly different after the yielding of the vessel material. The FEA analysis convergence could not be sustained after excessive deformation. The strain levels at the end of the convergence were not suitable to apply the double slope limit pressure method since the double slope line doesn't intersect the load deformation line. On the other hand, the tangent intersection is not useful because the plastic region of the multilinear curve is not mature whereas the plastic part of the bilinear curve reaches to horizontal line. Therefore, the limit pressure is taken to be the point of the end of the convergence. Figure 12 compared the pressure versus strain curves obtained through the FEA of the two material models.

To compare the multilinear isotropic hardening model strain behavior with the experimental results, rosette type strain gages were utilized to measure the local strains (axial and hoop) in the above-mentioned positions (Fig. 1). The axial and hoop strains obtained during the burst pressure tests were compared with the FEA results. Figure 13 shows the comparison of experimental and predicted strain values at the strain gages located at the front, central, and aft section of the vessel, respectively. It was found that the experimental and FEA results show good correlation. While the hoop strain behavior of the back cylindrical section of the pressure vessel was similar to the experimental results, there were

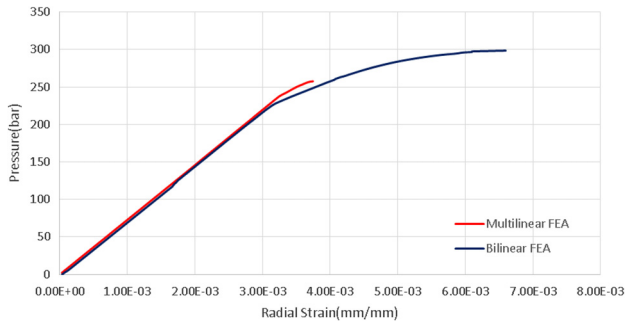

Fig. 12 Internal pressure versus radial strain for multilinear and bilinear model

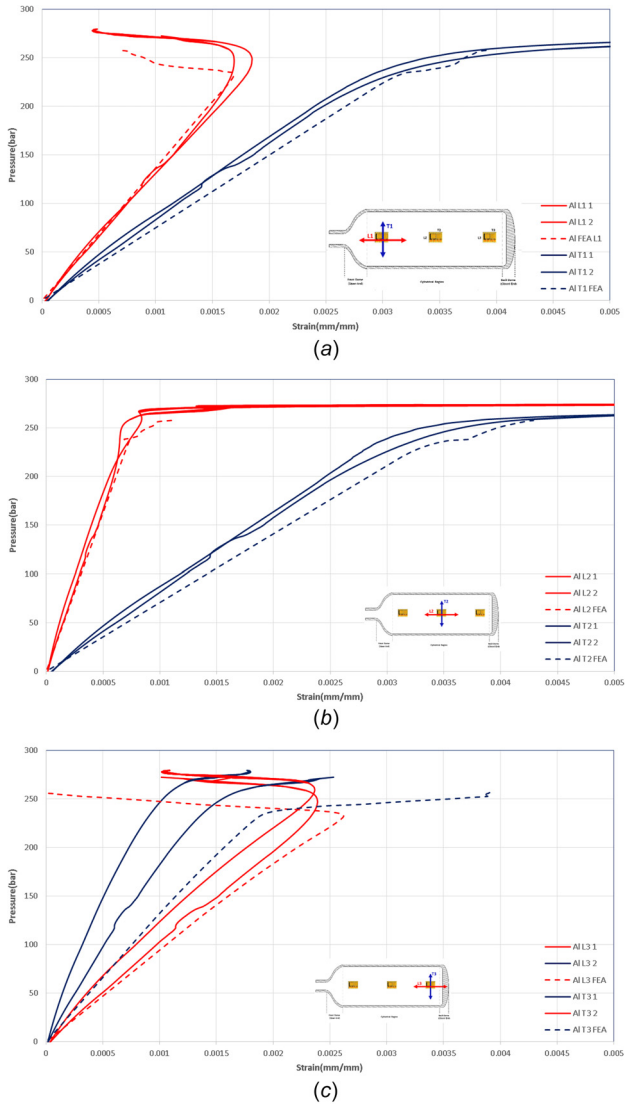

Fig. 13 A comparison of experimental and FEA prediction of axial and hoop strain values of the Al pressure vessel at (*a*) front, (*b*) central, and (*c*) back cylindrical section positions

still significant deviations in the strain values. This can be attributed to the local plastic deformation occurred at the back cylindrical section of that specific vessel.

Table 4 summarizes all burst pressure results calculated from different approaches. It should be noted that analytical results assumed that burst occurs immediately after yielding. Similarly, in FE analysis with the multilinear isotropic hardening material model, postnecking plastic behavior was omitted because of convergence problems encountered in that plastic region of the ductile metal.

Among elastoplastic analytical approaches, the theory based on the Tresca criterion underestimated the burst pressure while the formulae based on the von Mises criterion (von Mises-based, Svensson's formula and Christopher's approach) overestimated the failure pressure. The new analytical approach ASSC obtained the most accurate result compared to the experimental one. The tendency of overestimation of the elastoplastic approaches can be explained by the manufacturing flaws including the local formation of microcracks and thickness variations of vessels which are not considered in the analytical approaches and numerical simulations.

The FE analysis results underestimated the burst pressure with multilinear model and overestimated with the bilinear model, compared to experimental findings.

4 Concluding Remarks

In this paper, the mechanical response and burst pressure of Al-6061-T6 pressure vessel were determined by the combined usage of experimental, analytical, and numerical results. Analytical theories considering the elastic and plastic deformation of the Al liner were incorporated to predict the failure of cylindrical and dome sections of the vessel. In the numerical simulations, two different isotropic hardening models were utilized for defining the plastic region of the material, the bilinear, and multilinear isotropic hardening. The following conclusions can be drawn;

- The burst pressure based on the elastic stress approach for the cylindrical section was calculated as 224.5 bar with a relative error of −19.5% as compared to the experimental result, which was 279 bar. Although the elastic approach underestimated the burst failure, it correctly predicted the burst location. The elastic analysis provides a good preliminary basis for the limit load analysis for the pressure vessels.
- The theories based on plastic instability analysis significantly improved the burst pressure prediction so that there was a good agreement by using the ASSC approach with a relative error of only 2.2% and 285.1 bar with regard to the experimental result. Instead of using elastic stress analysis, the theories based on plastic instability should be used to determine the burst pressure correctly.
- The solution of the developed FE model provided the best burst failure prediction for the Al vessels. The solid model developed for the FE was found to be insensitive to the element mesh sizes.
- Two different approaches were utilized for determining the burst pressure from the FE analysis results. The mechanical behavior obtained from the tensile tests and supplied to the FE software. The error of the FE model was below 10%.
- It was also observed that experimentally obtained mechanical property input to the multilinear isotropic hardening material model in the FE software improved the accuracy of the strain behavior of the vessel with exception of postyielding part since the analysis was pressure controlled, whereas in the experiment with the increasing strains, the pressure level stays constant at some sections of the experiment.

Acknowledgment

This study was supported by TÜBİTAK (Scientific and Technical Research Council of Turkey) under project number of 215M182. The authors acknowledge this valuable support.

Funding Data

- Türkiye Bilimsel ve Teknolojik Araştirma Kurumu (No. 215M182; Funder ID: 10.13039/501100004410).

References

[1] Borel, J.-P., 1981, "Thermodynamical Size Effect and the Structure of Metallic Clusters," Surf. Sci., **106**(1–3), pp. 1–9.

[2] Barthelemy, H., Weber, M., and Barbier, F., 2017, "Hydrogen Storage: Recent Improvements and Industrial Perspectives," Int. J. Hydrogen Energy, **42**(11), pp. 7254–7262.

[3] San Marchi, C., Dedrick, D. E., Van Blarigan, P., Somerday, B. P., and Nibur, K. A., 2011, "Pressure Cycling of Type 1 Pressure Vessels With Gaseous Hydrogen," Fourth International Conference on Hydrogen Safety, Francisco CA, Sept. 12–14, pp. 1–12.

[4] Johns, R. H., and Kaufman, A., 1967, "Filament-Overwrapped Metallic Cylindrical Pressure Vessels," AIAA Paper No. 28981.

[5] Kabir, M. Z., 2000, "Finite Element Analysis of Composite Pressure Vessels With a Load Sharing Metallic Liner," Compos. Struct., **49**(3), pp. 247–255.

[6] Shibley, A. M., 1982, "Filament Winding," G. Lubin, ed., Handbook of Composites, Springer, Berlin.

[7] Magneville, B., Gentilleau, B., Villalonga, S., Nony, F., and Galiano, H., 2015, "Modeling, Parameters Identification and Experimental Validation of Composite Materials Behavior Law Used in 700 Bar Type IV Hydrogen High Pressure Storage Vessel," Int. J. Hydrogen Energy, **40**(38), pp. 13193–13205.

[8] Berro Ramirez, J. P., Halm, D., Grandidier, J.-C., Villalonga, S., and Nony, F., 2015, "700 Bar Type IV High Pressure Hydrogen Storage Vessel Burst—Simulation and Experimental Validation," Int. J. Hydrogen Energy, **40**(38), pp. 13183–13192.

[9] Moskvichev, E., 2016, "Numerical Modeling of Stress-Strain Behavior of Composite Overwrapped Pressure Vessel," Procedia Struct. Integr., **2**, pp. 2512–2518.

[10] Zheng, J. Y., and Liu, P. F., 2008, "Elasto-Plastic Stress Analysis and Burst Strength Evaluation of Al-Carbon Fiber/Epoxy Composite Cylindrical Laminates," Comput. Mater. Sci., **42**(3), pp. 453–461.

[11] Liu, P. F., and Zheng, J. Y., 2008, "Progressive Failure Analysis of Carbon Fiber/Epoxy Composite Laminates Using Continuum Damage Mechanics," Mater. Sci. Eng. A, **485**(1–2), pp. 711–717.

[12] Zhu, X.-K., and Leis, B. N., 2012, "Evaluation of Burst Pressure Prediction Models for Line Pipes," Int. J. Pressure Vessel Piping, **89**, pp. 85–97.

[13] Liu, P. F., Xing, L. J., and Zheng, J. Y., 2014, "Failure Analysis of Carbon Fiber/Epoxy Composite Cylindrical Laminates Using Explicit Finite Element Method," Compos. Part B, **56**, pp. 54–61.

[14] Zhu, X.-K., and Leis, B. N., 2004, "Strength Criteria and Analytic Predictions of Failure Pressure in Line Pipes," Int. J. Offshore Polar Eng., **14**(2), pp. 125–131.

[15] Dill, E. H., 2011, *The Finite Element Method for Mechanics of Solids With ANSYS Applications*, 1st ed., CRC Press, Boca Raton, FL.

[16] Ling, Y., 1996, "Uniaxial True Stress-Strain After Necking," AMP J. Technol., **5**, pp. 37–48.

[17] Yao, D., Cai, L., and Bao, C., 2016, "A New Approach on Necking Constitutive Relationships of Ductile Materials at Elevated Temperatures," Chin. J Aeronaut., **29**(6), pp. 1626–1634.

[18] Liu, P. F., and Zheng, J. Y., 2010, "Finite Element Analysis of Tensile Behavior of Ductile Steel With Defects," J. Fail Anal. Prev., **10**(3), pp. 212–217.

[19] Huang, X., Chen, Y., Lin, K., Mihsein, M., Kibble, K., and Hall, R., 2007, "Burst Strength Analysis of Casing With Geometrical Imperfections," ASME J. Pressure Vessel Technol., **129**(4), pp. 763–770.

[20] Paul, S. K., Roy, S., Sivaprasad, S., Bar, H. N., and Tarafder, S., 2018, "Identification of Post-Necking Tensile Stress–Strain Behavior of Steel Sheet: An Experimental Investigation Using Digital Image Correlation Technique," J. Mater Eng. Perform., **27**(11), pp. 5736–5743.

[21] Tardif, N., and Kyriakides, S., 2012, "Determination of Anisotropy and Material Hardening for Aluminum Sheet Metal," Int. J. Solids Struct., **49**(25), pp. 3496–3506.

[22] Barlat, F., Aretz, H., Yoon, J. W., Karabin, M. E., Brem, J. C., and Dick, R. E., 2005, "Linear Transformation-Based Anisotropic Yield Functions," Int. J. Plast., **21**(5), pp. 1009–1039.

[23] Korkolis, Y. P., Kyriakides, S., Giagmouris, T., and Lee, L.-H., 2010, "Constitutive Modeling and Rupture Predictions of Al-6061-T6 Tubes Under Biaxial Loading Paths," ASME J. Appl. Mech., **77**, p. 064501.

[24] Xue, L., Widera, G. E. O., and Sang, Z., 2007, "Burst Pressure Prediction of Cylindrical Shell Intersection," SMiRT 19, Toronto, ON, Canada, Aug. 12–17, pp. 1–8.

[25] Brabin, T. A., Christopher, T., and Nageswara Rao, B., 2011, "Bursting Pressure of Mild Steel Cylindrical Vessels," Int. J. Pressure Vessel Piping, **88**(2–3), pp. 119–122.

[26] Cho, Y., and Kim, T., 2016, "Estimation of Ultimate Strength in Single Shear Bolted Connections With Aluminum Alloys (6061-T6)," Thin-Walled Struct., **101**, pp. 43–57.

[27] ASTM International, 2016, "Standard Test Methods for Tension Testing of Metallic Materials," ASTM, West Conshohocken, PA, Standard No. ASTM E8/E8M-16a.

[28] Zhu, X.-K., and Leis, B. N., 2005, "Influence of Yield-to-Tensile Strength Ratio on Failure Assessment of Corroded Pipelines," ASME J. Pressure Vessel Technol., **127**(4), pp. 436–442.

[29] Zhu, X.-K., and Leis, B. N., 2007, "Theoretical and Numerical Predictions of Burst Pressure of Pipelines," ASME J. Pressure Vessel Technol., **129**(4), pp. 644–652.

[30] Christopher, T., Rama Sarma, B. S., Govindan Potti, P., Nageswara Rao, B., and Sankarnarayanasamy, K., 2002, "A Comparative Study on Failure Pressure Estimations of Unflawed Cylindrical Vessels," Int. J. Pressure Vessel Piping, **79**(1), pp. 53–66.

[31] Moss, D., and Basic, M., 2013, *Pressure Vessel Design Manual*, 4th ed., Elsevier, Oxford, UK.

[32] Zhang, Z., Sun, Q., Li, C., and Zhao, W., 2006, "Theoretical Calculation of the Strain-Hardening Exponent and the Strength Coefficient of Metallic Materials," J. Mater. Eng. Perform., **15**(1), pp. 19–22.

[33] Ansys, Inc., 2007, "Theory Reference for ANSYS and ANSYS Workbench," ANSYS Release User Manual, 11.0th ed., Ansys, Canonsburg, PA.

[34] Ansys, Inc., 2013, "Mechanical APDL Programmer's Reference, Release 15.0," Ansys, Canonsburg, PA.

[35] Mackenzie, D., and Li, H., 2006, "A Plastic Load Criterion for Inelastic Design by Analysis," ASME J. Pressure Vessel Technol., **128**(1), pp. 39–45.